



Figures and figure supplements

Anti-ferroptotic mechanism of IL4i1-mediated amino acid metabolism

Leonie Zeitler et al

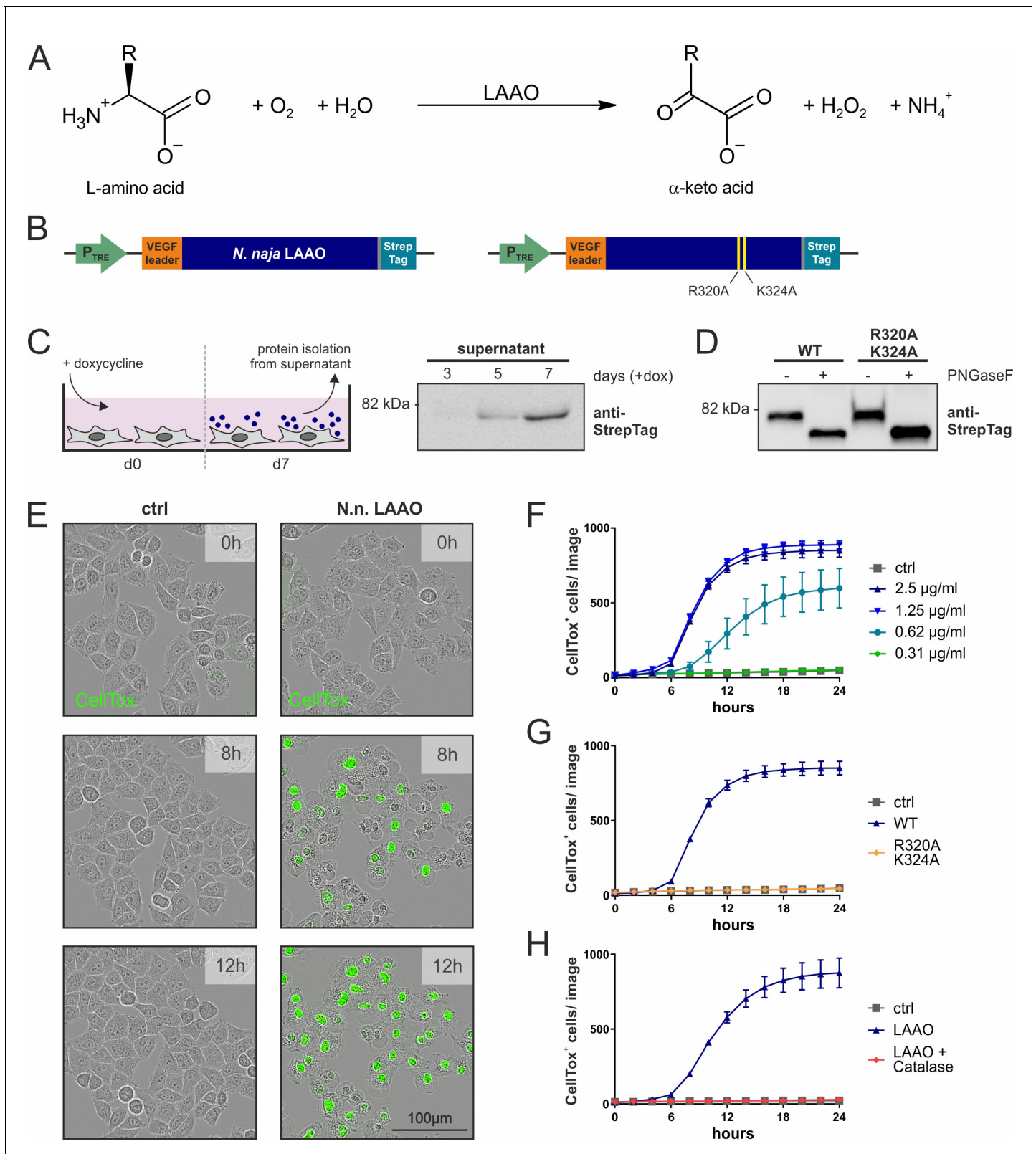


Figure 1. *Naja naja* LAAO is cell-lethal via H₂O₂. (A) Reaction mechanism of L-amino acid oxidases (LAAOs). (B) Construct design to express venom LAAOs in mammalian cells. The *N. naja* LAAO variants contain the human VEGF signal sequence and a C-terminal Strep-tag to facilitate purification. Mutations R320A and K324A ablate catalytic activity. (C) Purification strategy for LAAO, which is isolated from the cell supernatant. (D) Immunoblotting of purified recombinant proteins. LAAO or the enzyme-dead variant are glycosylated in their secreted forms. (E) Representative microscopy images of Figure 1 continued on next page

Figure 1 continued

HeLa cells stained with the cell death dye CellTox following addition of 2.5 $\mu\text{g/ml}$ *N. naja* LAAO. (F) Quantification of cell death across time induced by *N. naja* LAAO. (G) *N. naja* LAAO R320A and K324A enzyme-dead version fails to induce death. 2.5 $\mu\text{g/ml}$ of WT and mutant enzyme was added. (H) Addition of catalase (25 $\mu\text{g/ml}$) blocks cell death induced by *N. naja* LAAO (2.5 $\mu\text{g/ml}$). (F–H): $n = 3$ biological replicates; the graphs are representative for three independent experiments. All error bars represent standard deviation.

A

C. rhodostoma	1	MNVFFMFSLFLA-----ALGSCADDRNPLAECFOENDYEEFLEIARNGLKATSNPK
N. naja	1	-----DDRRSPLEECFOONDYEEFLEIARNGLKKTSNPK
M. musculus	1	MAGLALRI-VLAATLLGLAGSLDWAASSLNPTKCMEDHDYEQLKVVTLGLNRTSKPQ
H. sapiens	1	MAPLALHLLVLPILLSLVASQDWAERSQDFEKCMQDPDYEQLKVVVTWGLNRTLKPKQ
C. rhodostoma	53	HVVIIVGAGMAGLSAAYVLAGAGHQVTVLEASERPGGRVRYTYRNEEAGWYANLGPMLRPEK
N. naja	35	HVVVVGAGMAGLSAAYVLAGAGHKVTLLEASERVGGRVVTYHNDREGWYVNMGPMLRPER
M. musculus	60	KVVVVGAGVAGLVAAKMLSDAGHKVTILEADNRIGRIIFTFRDEKTIWICELGAMRMPS
H. sapiens	61	RVTIIVGAGVAGLVAAKVLSDAGHKVTILEADNRIGRIIFTYRDQNTGWICELGAMRMPS
C. rhodostoma	113	HRIVREYIRKFDLRLNEFSQENDNAWYFIKNIIRKKVGEVKKDEGLKYPVKPSEACKSAG
N. naja	95	HRIVREYIRKFGKLNNEFFQENENAWYYINNIIRKRVWEVKKDPSLKYVPKPSSEEGKSAS
M. musculus	120	HRILHKLCRTLGLNLTQFTQYDENTWTEVHNVKLRNYVVEKMPKLGYNLNNRERGHSP
H. sapiens	121	HRILHKLCQGLGLNLTQFTQYDKNWTEVHEVKLRNYVVEKVPKLGVALRPOEKGHSP
C. rhodostoma	173	QLYEESLGVVEELKRTNCSYIILNKYDYSTKTYLKEGDLSPGAVDMIGDLLNEDSGY
N. naja	155	QLYQESLGRVIEELKRTNCSYIILSKYDYSYTKTYLKEGNLSRGAVDMIGDLLNEDSSYH
M. musculus	180	DIYQMALNKAFKDLKALGCKKAMNKNKHTLLEYLLEGNLSRPAVQLLGDVMSEEGFFY
H. sapiens	181	DIYQMALNQALKDLKALGCRKAMKKFERHTLLEYLLEGNLSRPAVQLLGDVMSEEGFFY
C. rhodostoma	233	VSFIESLKHDDIFAYEKRFDEIVDGMCKLPTAMYRDIQDKVHFNAQVIKIQONDQKVTIV
N. naja	215	LSFIESLKSDFLFSYEKRFDEIVGGFDQLPISMYQAIETVHLNARVTKIQYDAEKVRVT
M. musculus	240	LSFAEALRAHACLSDRLRYSRIVGGWDLPRALLSSLGALLLNAPVVSITQGRNDVVRH
H. sapiens	241	LSFAEALRAHSCLSDRLOYSRIVGGWDLPRALLSSLGSLVLLNAPVAVMTQGPVHVH
C. rhodostoma	293	YE-T-LSKETPVSVDADYVIVCTTSRAVRLIKFNPLLPKKAHALRSVHYSGTKIFLTC
N. naja	275	YQ-T-PAKTF--VTADYVIVCSTSRARRIYFEPLEPKKAHTLRSIHYSGTKIFLTC
M. musculus	300	IATSLH--SEKTLTADVLLTASGPALQRITFSPLTRKROEALRALHYVAASKVFLSFR
H. sapiens	301	IETSPPARNLKVLKADVLLTASGPAVKRITFSPLERHMQEALRLHYVPATKVFLSFR
C. rhodostoma	351	TKFEWEDDGIHGGKSTTDLPSEFTIYPNHNFTNGVGVIIAYGIGDDANFFQALDFKDCADI
N. naja	331	KKFEWADGIHGGKSTTDLPSEFTIYPNHNFTTIGVIMAYVLADDSDFFQALDTKTCADI
M. musculus	358	RPFWHEEHEGGHSNTDRPSRILFYPARG--EGSLLLASYTWSDAAPAEAGLSTDTLRL
H. sapiens	361	RPFWREHEHEGGHSNTDRPSRMLFYPPR--EGALLASYTWSDAAPAEAGLSREEARL
C. rhodostoma	411	VFNDLSLIHQLEKKDIQSFVSVIQQKWSLDKYAMCGITTFTPYQFQHFSD-PLTASQGR
N. naja	391	VINDLSLIHQLEKREIQALCYP-SIKKWNLDKYTMGSITSFTPYQFQDYFE-SAAAPVGR
M. musculus	416	VLDVAALHGP-V-VFRLWDGRGVVWRWAEDPHSQGGFVVOPPLYGREAEDYDWSAPFGR
H. sapiens	419	ALDDVAALHGP-V-VRLWDGTGVVWRWAEDQHSQGGFVVOPPALWQTEKD-DWTVVYGR
C. rhodostoma	470	IYFACEYTAQAHGWIDSTIKSGLRAARDVNLA---SENPSCGTHLSNDNE-----
N. naja	449	IHFAGEYTGREHGWIDSTIMTGLRAARDVNRA---SQKPSKIRLISDNQ-----
M. musculus	474	IYFACEHTALPHGWVETAVKSGLRAAVRINNNYGYGEVDPQMMEHYAEANYLDQYPEGE
H. sapiens	476	IYFACEHTAYPHGWVETAVKSSALRAAIKINSRKGASDTASPEGHASDMEGQGHVHGVS
C. rhodostoma	516	-----
N. naja	495	-----
M. musculus	534	RPEEQQAREEVSPDEQEP SHKLLVETSPEGQQAHFVEAIPELQGHVVFVETVPQEKGH
H. sapiens	536	-----SPSHDLAKEEGSHPPVQGLSLQ-----
C. rhodostoma	516	-----L
N. naja	495	-----L
M. musculus	594	QNIYPSEHVQVHGEVPEWHGEGGSGTPQMHRVGDHS
H. sapiens	559	-----NTTTRTS-----H

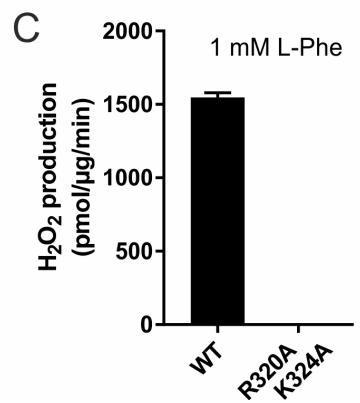
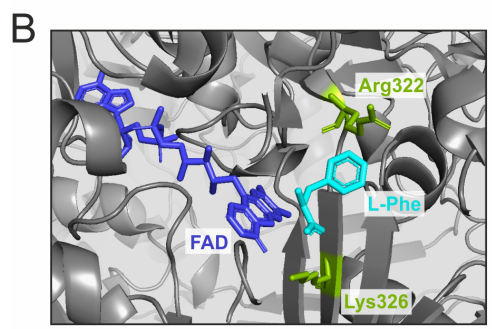


Figure 1—figure supplement 1. *Naja naja* LAAO is cell-lethal via H₂O₂. (A) Multiple sequence alignment of *Calloselasma rhodostoma*, *N. naja*, LAAO, and *Mus musculus* and *Homo sapiens* IL4i1. Sites displayed in green represent residues used to generate enzyme-dead point mutants. (B) Figure 1—figure supplement 1 continued on next page

Figure 1—figure supplement 1 continued

Representative structure of the catalytic domain of *C. rhodostoma* LAAO (PDB: 2IID) with co-factor FAD and substrate L-Phe. The conserved residues mutated in the *N. naja* enzyme-dead version are displayed in green. (C) LAAO WT and enzyme-dead variant activity, quantified as H₂O₂ production, with 1 mM of L-Phe as substrate (n = 3 technical replicates). Error bars represent standard deviation.

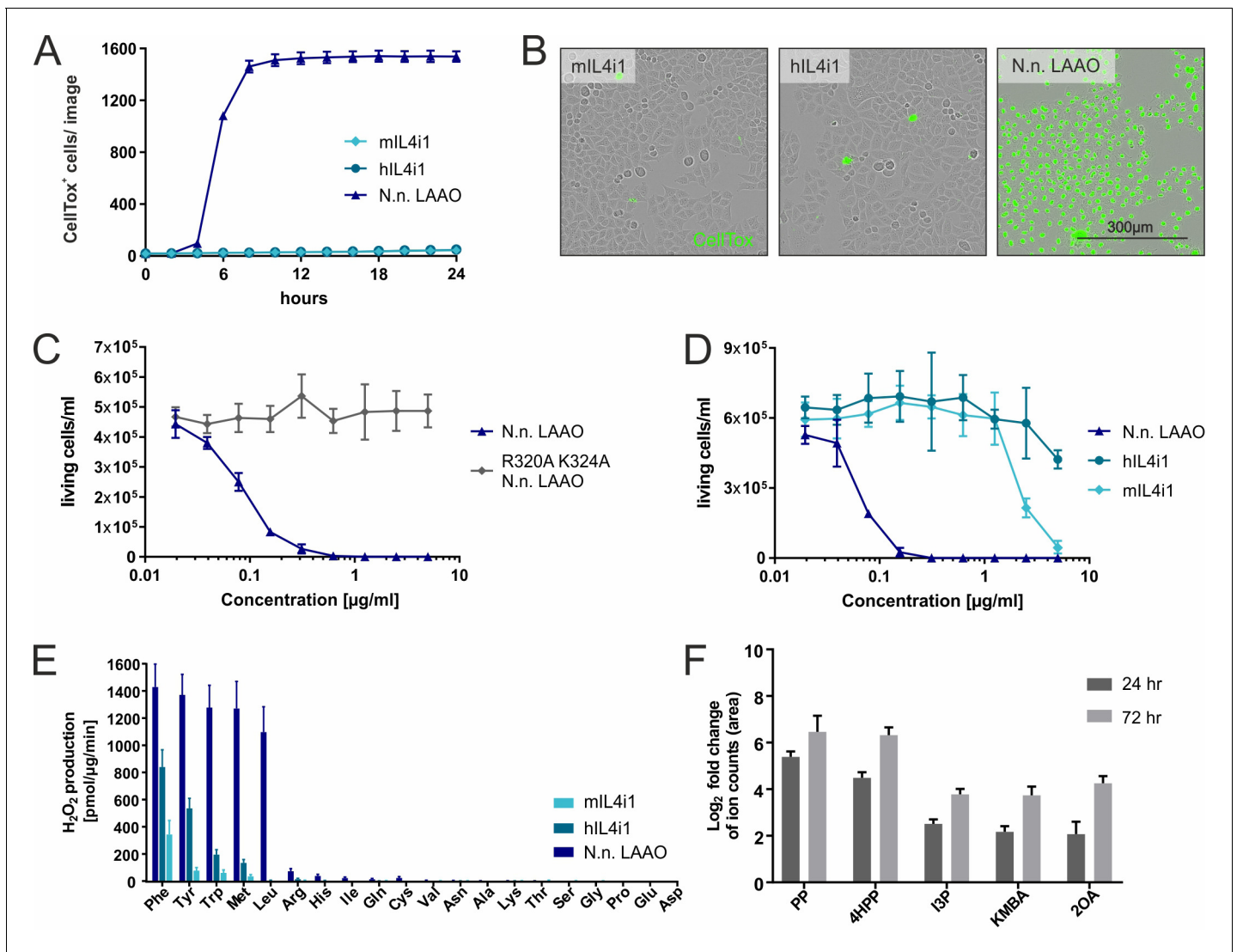


Figure 2. Substrate ranges and properties of IL4i1 compared to LAAO. (A) Human or mouse IL4i1 fail to induce cell death of HeLa cells at equivalent concentrations to *Naja naja* LAAO (all enzymes added at 2.5 µg/ml) (n = 3 biological replicates). (B) Representative microscopy images with CellTox staining from an experiment similar to that in (A). (C) Activity of *N. naja* LAAO or its enzyme-dead mutant to RS4;11 human leukemia cells. 1 × 10⁴ cells were plated in round-bottom 96-well plates and treated with the indicated concentrations of LAAO enzyme. The final viable cell number was determined 72 hr after treatment (n = 3 biological replicates). (D) As in (C) comparing human and mouse IL4i1 to *N. naja* LAAO (n = 4 biological replicates). (E) Comparative enzyme activity of human and mouse IL4i1 versus *N. naja* LAAO using single amino acids. The graph includes three independent experiments. (F) Log₂-fold change of ion counts compared to untreated medium of significantly increased amino acid metabolites (p < 0.01) detected by untargeted metabolomics in DMEM incubated for 24 or 72 hr with 1 µg/ml of human IL4i1; n = 3 biological replicates. All error bars represent standard deviation.

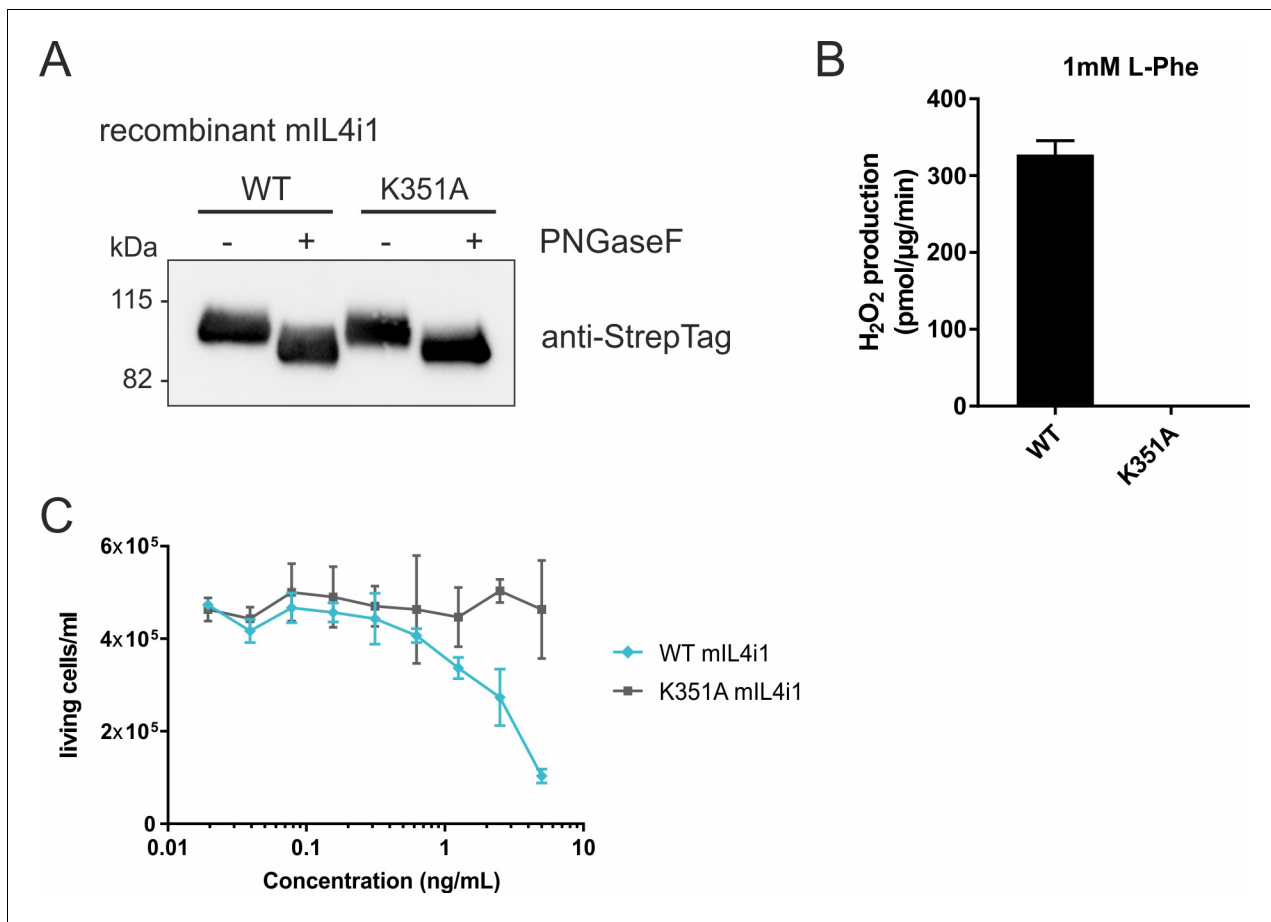


Figure 2—figure supplement 1. Substrate ranges and properties of IL4i1 compared to LAAO. (A) Recombinant murine IL4i1 and the enzyme-dead variant are glycosylated in their secreted forms. (B) WT and mutant murine IL4i1 activity, quantified by H₂O₂ production with 1 mM of L-Phe as substrate (n = 3 technical replicates). (C) Cell viability of RS4;11 human leukemia cells in the presence of murine IL4i1 or its enzyme-dead mutant. 1 × 10⁴ cells were plated in round-bottom 96 well plates and treated with the indicated concentrations of IL4i1 enzyme. The final viable cell number was determined 72 hr after treatment (n = 3 biological replicates). All error bars represent standard deviation.

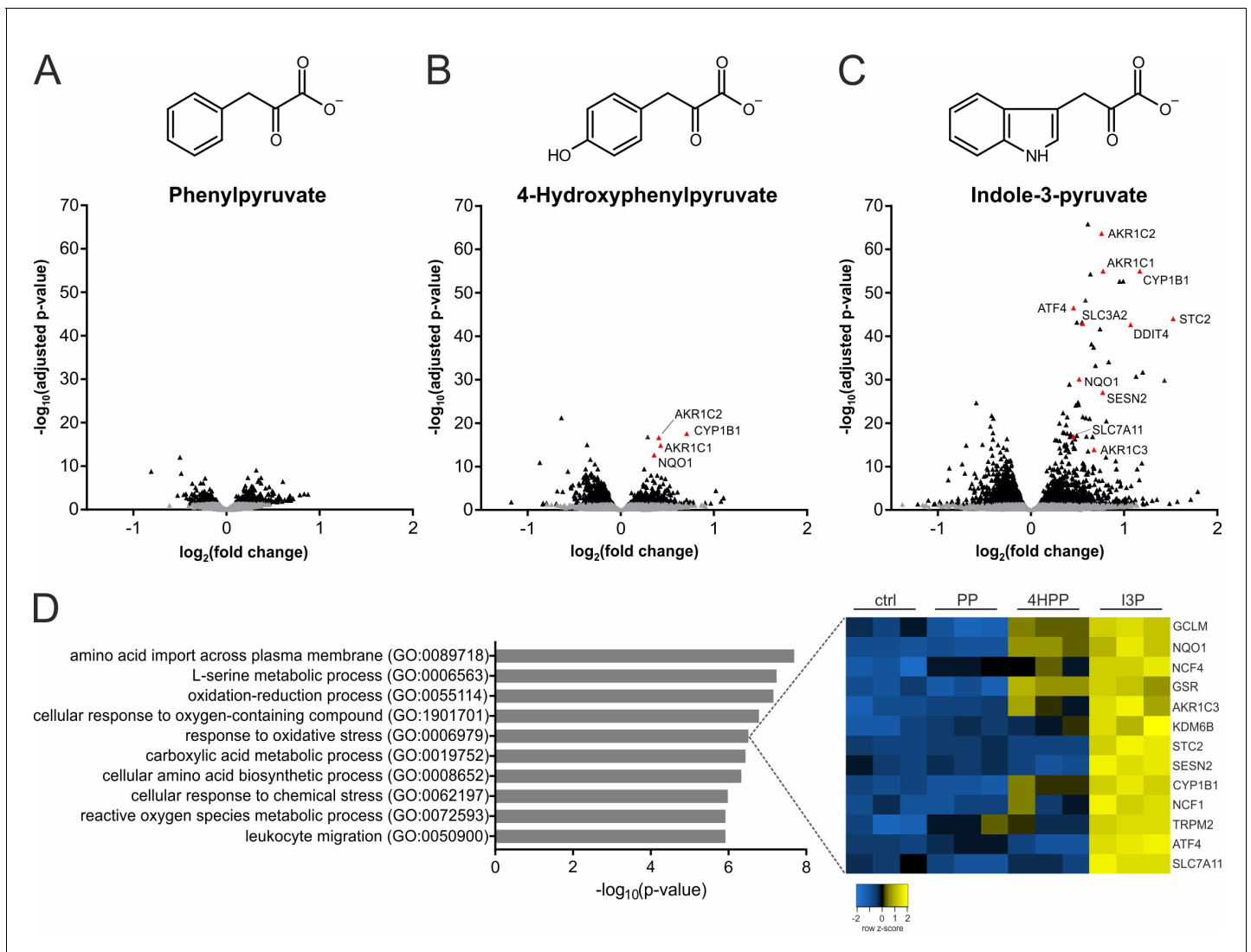


Figure 3. IL4i1 products induce specific stress and redox-protective gene expression programs. (A–C) THP-1 human monocytic cells were treated for 24 hr with PP, 4HPP, or I3P (200 μ M) and RNAseq analysis was used to quantify gene expression changes compared to untreated controls. (D) Top hits of GO term overrepresentation analysis of the most significantly (p -value cutoff $p < 10^{-5}$) upregulated genes by I3P treatment (left). The full table of significant GO terms is provided (**Supplementary file 1**). Heat map of genes detected in the analysis under the term GO:0006979 (right).

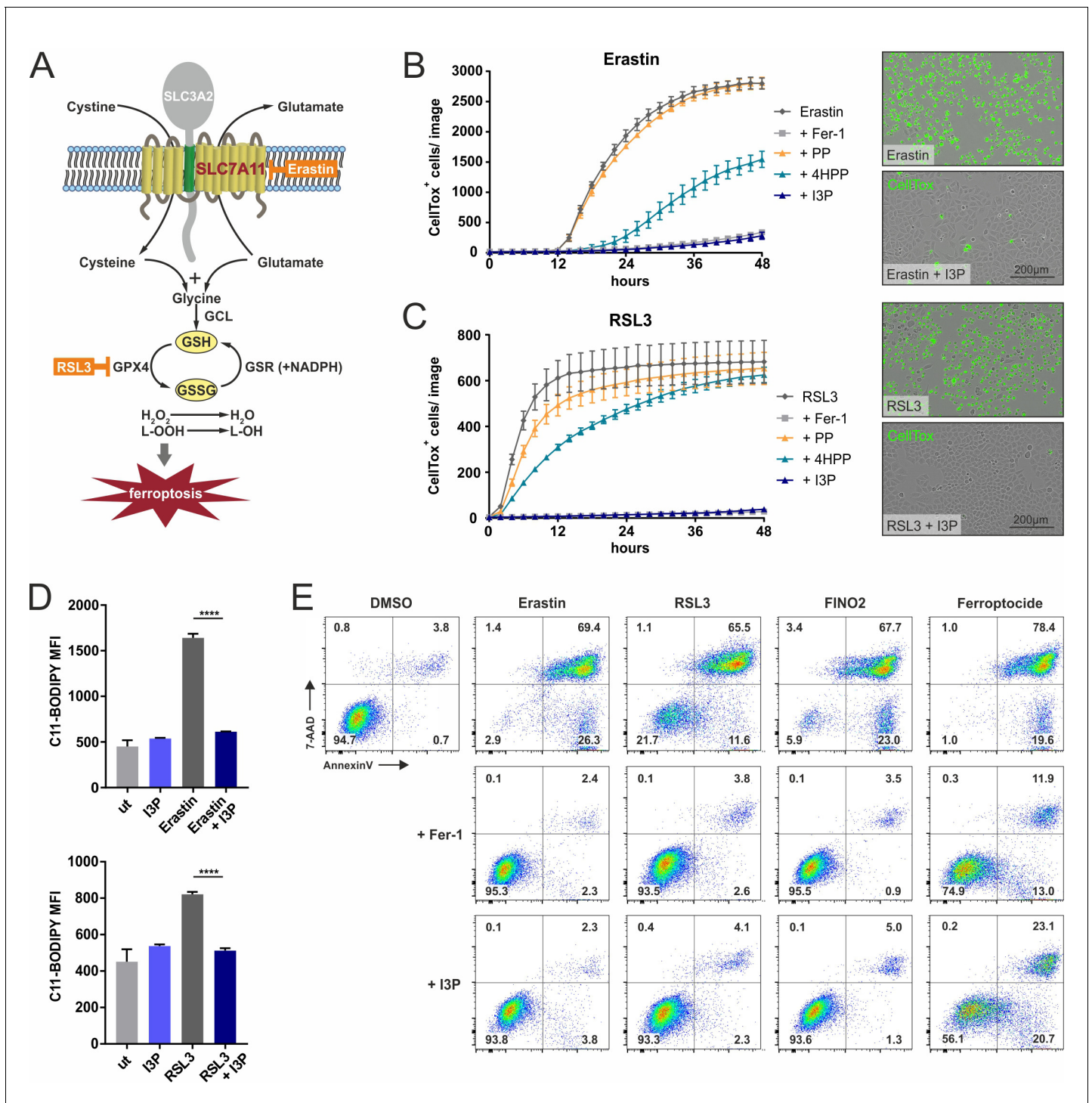


Figure 4. IL4i1 metabolites form an anti-ferroptotic hierarchy. (A) Simplified schema of ferroptosis control showing the points of chemical perturbation by erastin and RSL3. (B) Quantification of cell death of HeLa cells treated with the ferroptosis inducer erastin in the presence of 200 μ M PP, 4HPP, or I3P by live cell imaging using CellTox staining. Ferrostatin-1 (Fer-1) was added as a control to block erastin-induced death and has an equivalent suppressing effect as I3P. Right panel, representative CellTox staining images from an experiment similar to (B). (C) As in B, using RSL3 to induce ferroptosis. B,C: n = 3 biological replicates. The graphs are representative for three independent experiments. (D) I3P blocks lipid peroxidation induced by erastin and RSL3 determined by flow cytometry using C11-BODIPY. n = 3 biological replicates; data were analyzed by one-way ANOVA with Tukey's multiple comparisons test; ****p<0.0001. All error bars represent standard deviation. (E) Flow cytometry analysis of the anti-ferroptotic activity of I3P (200 μ M) using Fer-1 as positive control. Murine NIH3T3 cells were treated with erastin, RSL3, FINO2, or ferropticide to induce ferroptosis in the absence or presence of Fer-1 or I3P and death quantified by 7-AAD and Annexin-V staining. See 'Materials and methods' for details of reagent concentrations and timing. The plots are representative for two independent experiments.

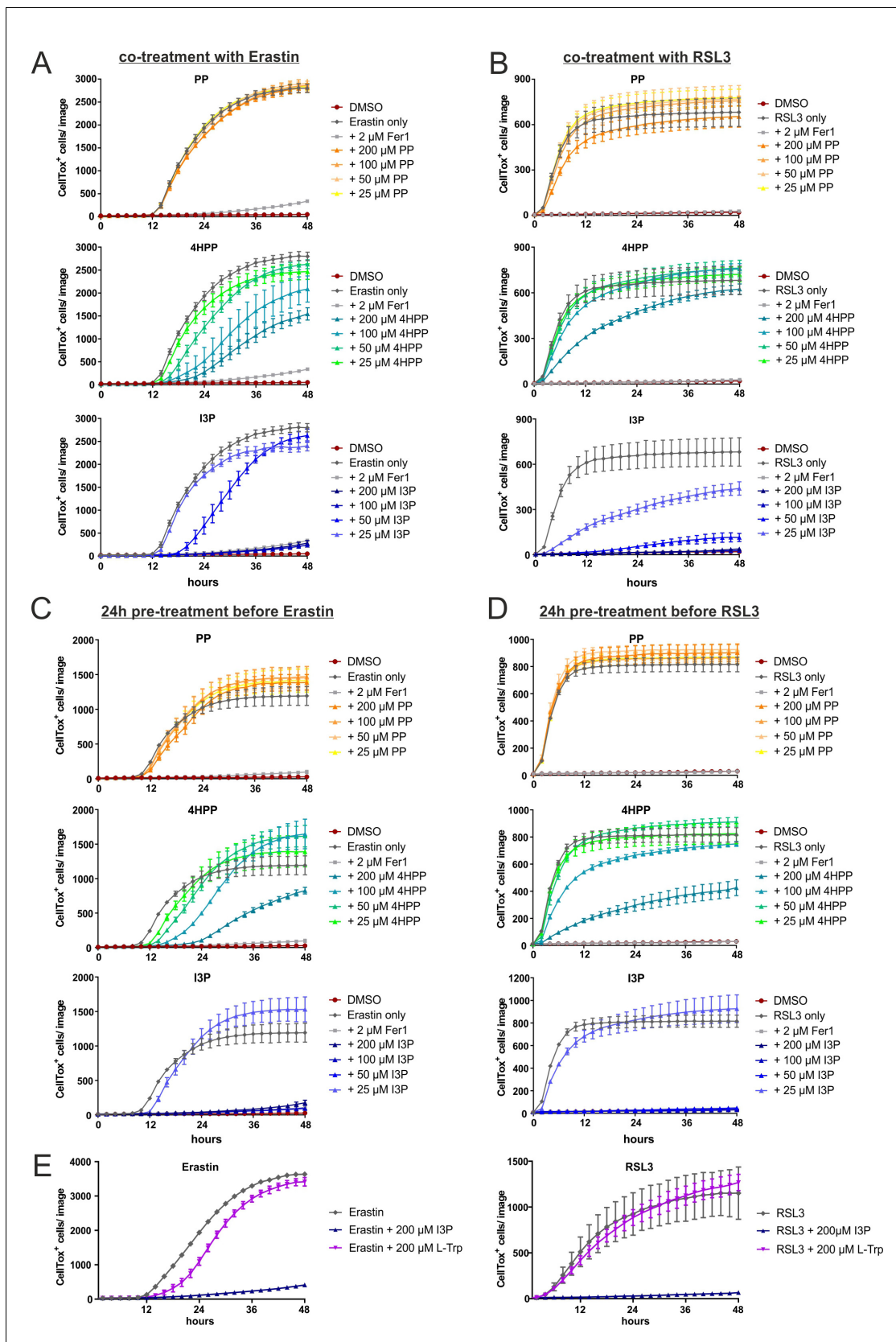


Figure 4—figure supplement 1. IL4i1 metabolites form an anti-ferroptotic hierarchy. (A) HeLa cells were concurrently treated with erastin in the presence of increasing doses of PP, 4HPP, or I3P and death quantified over time using Incucyte imaging of CellTox staining. Ferrostatin-1 was added. *Figure 4—figure supplement 1 continued on next page*

Figure 4—figure supplement 1 continued

as a control. (B) As in (A), but using RSL3 to induce ferroptosis. (C) As in (A), but with 24 hr pre-treatment with the keto-acids before inducing ferroptosis with erastin. (D) As in (C), using RSL3 to induce ferroptosis. (E) HeLa cells were concurrently treated with erastin or RSL3 in the presence of 200 μ M L-Trp, 200 μ M I3P, or control DMEM medium. All experiments: n = 3 biological replicates; the graphs are representative for three independent experiments. All error bars represent standard deviation.

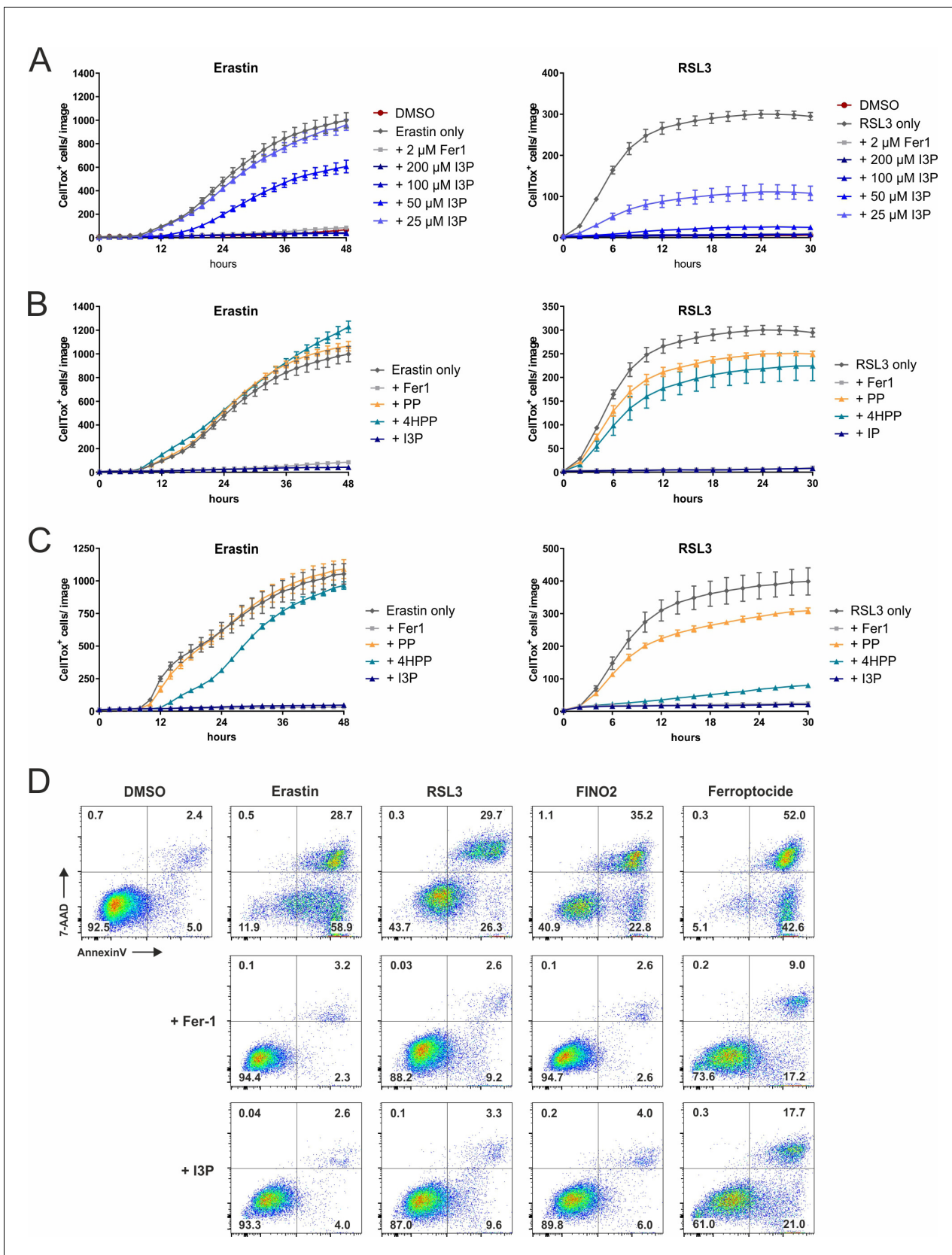


Figure 4—figure supplement 2. IL4i1 metabolites form an anti-ferroptotic hierarchy. (A) HT1080 cells were concurrently treated with erastin (left) and RSL3 (right) in the presence of increasing doses of I3P and death quantified over time using Incucyte imaging of CellTox staining. Ferrostatin-1 was Figure 4—figure supplement 2 continued on next page

Figure 4—figure supplement 2 continued

added as a control. **(B)** As in **(A)**, comparing 200 μ M of PP, 4HPP, and I3P. **(C)** As in **(B)**, but with 24 hr of pre-treatment with the keto-acids before inducing ferroptosis. A–C: $n = 3$ biological replicates. The graphs are representative for two independent experiments. All error bars represent standard deviation. **(D)** Flow cytometry analysis of the anti-ferroptotic activity of I3P (200 μ M) using Fer-1 as positive control. HT1080 cells were treated with erastin, RSL3, FINO2, or ferroptocid to induce ferroptosis in the absence or presence of ferrostatin or I3P and death quantified by 7-AAD and Annexin-V staining. The plots are representative for two independent experiments.

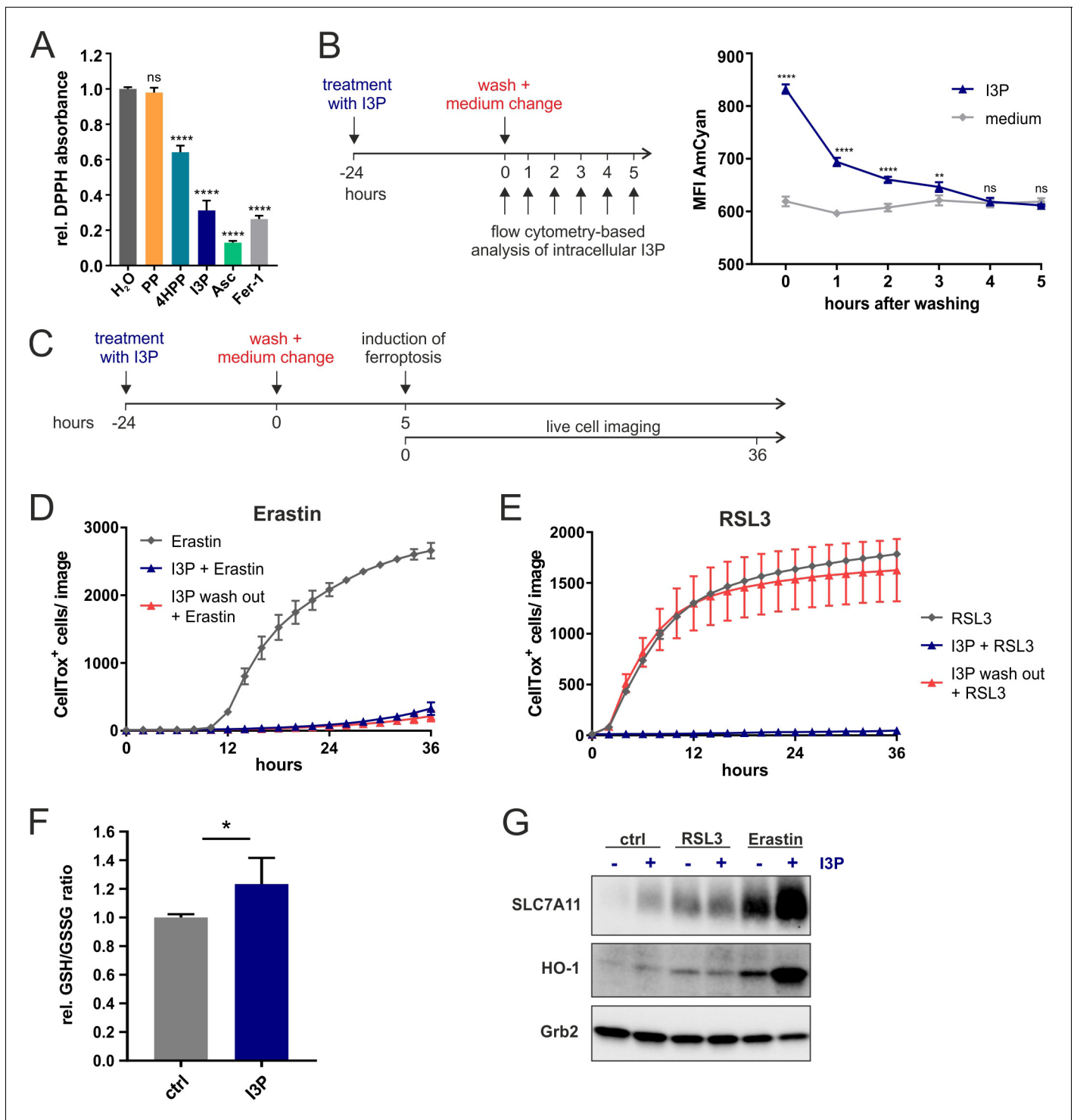


Figure 5. Anti-ferroptotic mechanisms of I3P. (A) Cell-free scavenging activity of 200 μ M PP, 4HPP, I3P, ascorbic acid (Asc), and Fer-1 determined by changes in the absorbance at 517 nm of the stable radical DPPH relative to H₂O control. $n = 4$ Technical replicates; the graphs are representative for three independent experiments. Data were analyzed by one-way ANOVA with Dunnett's multiple comparisons test; **** $p < 0.0001$; ns = not significant. (B) Design of a wash-out experiment to quantify intracellular I3P. HeLa cells were incubated for 24 hr with or without 200 μ M I3P. After washing-out the I3P-containing medium, remaining intracellular I3P was determined by flow cytometry at the indicated time points. $n = 3$ biological replicates; the graphs are representative for three independent experiments. Data were analyzed by two-way ANOVA with Sidak's multiple comparisons test; ** $p < 0.01$; **** $p < 0.0001$; ns = not significant. (C) Adaptation of the assay in (B) to quantify direct versus indirect protective effects of I3P. (D) I3P retains protective activity against erastin-induced ferroptosis after wash-out. (E) I3P only protects against RSL3-induced ferroptosis if present in cells during the

Figure 5 continued on next page

Figure 5 continued

time of GPX4 inhibition. D,E: n = 2 biological replicates; the graphs are representative for three independent experiments. (F) GSH/GSSG ratio in HeLa cells treated with 200 μ M I3P for 24 hr relative to untreated control. n = 4 biological replicates; data were analyzed using an unpaired t-test; *p<0,05. All error bars represent standard deviation. (G) I3P induces the expression of SLC7A11 and HO-1 at protein level. HeLa cells were treated with I3P in the absence or presence of erastin or RSL3 for 24 hr and SLC7A11 and HO-1 levels determined by immunoblotting. Grb2 was used as loading control.

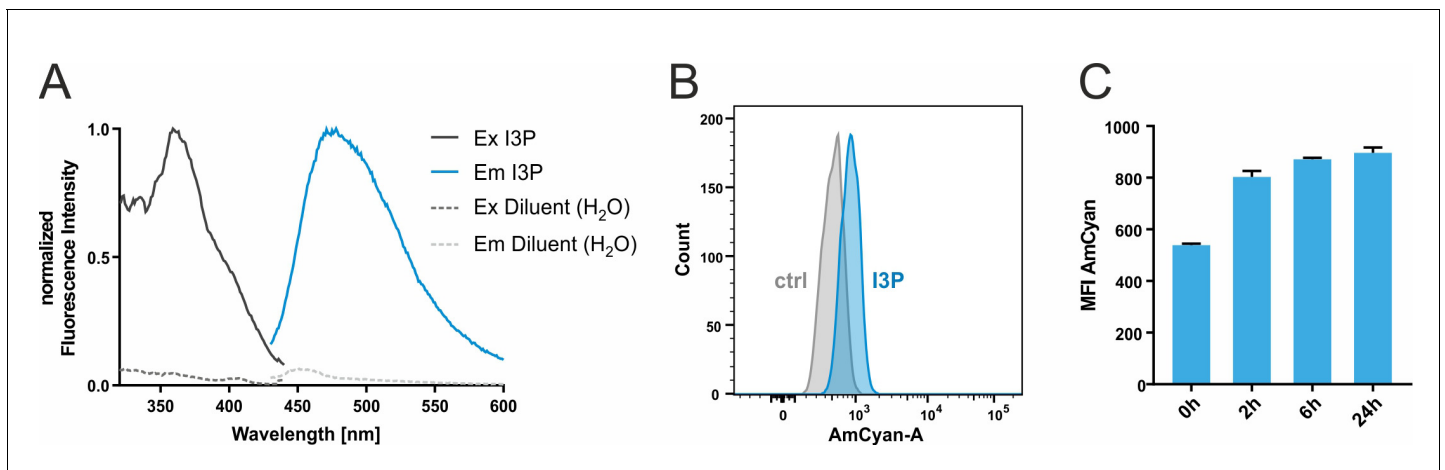


Figure 5—figure supplement 1. Anti-ferroptotic mechanisms of I3P. (A) Absorption (grey line) and emission (light blue line) spectra of I3P in neutral aqueous solution. (B) Flow cytometric evaluation of I3P uptake (200 μ M, 24 hr) by HeLa cells. Data acquired using 405 nm violet laser. (C) HeLa cells were treated with 200 μ M of I3P and 2, 6, and 24 hr and I3P uptake monitored by flow cytometry analyzing the mean fluorescence intensity in the AmCyan channel. $n = 3$ biological replicates; the graph is representative for three independent experiments. Error bars represent standard deviation.

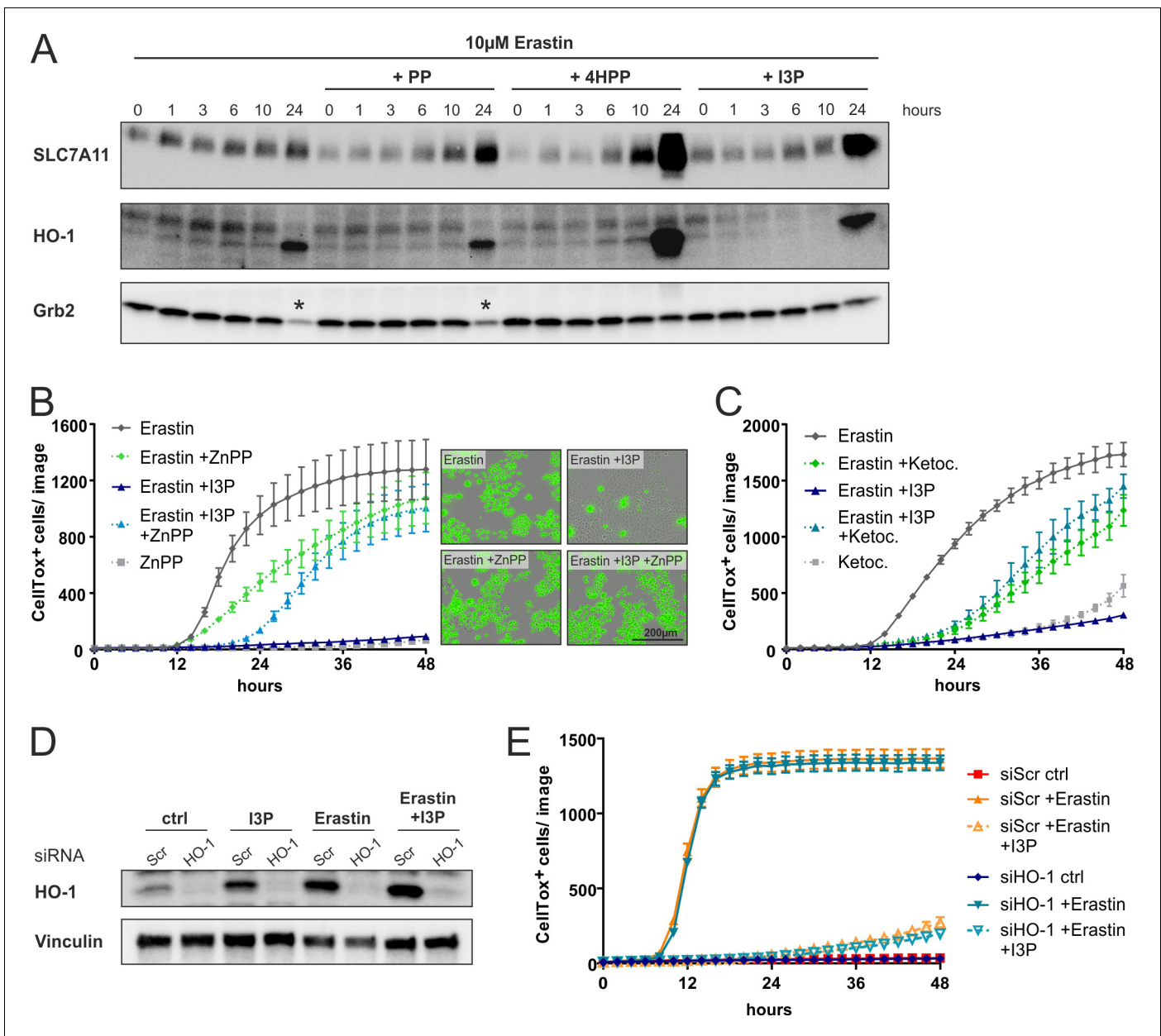


Figure 5—figure supplement 2. Anti-ferroptotic mechanisms of I3P. (A) I3P and 4HPP induce the expression of SLC7A11 and HO-1 at protein level. HeLa cells were treated with erastin in the presence of 200 μM of PP, 4HPP, and I3P for the indicated time and SLC7A11 or HO-1 protein levels were determined by immunoblotting; * indicates less protein amount due to cell death. (B) ZnPP (light blue triangles) interferes with the protective effects of I3P against erastin-induced ferroptosis. HeLa cells were treated with erastin in presence or absence of I3P with or without 10 μM of ZnPP and cell death quantified by CellTox Incucyte imaging. n = 2 biological replicates; the graph is representative for three independent experiments. Right: representative images of CellTox staining. (C) As in (B) using 100 μM ketoconazole. (D) Immunoblotting of HO-1 in cells transfected with 50 nM siRNA (siScr negative ctrl or siHO-1). Cells were lysed 15 hr after treatment with 200 μM I3P, 10 μM erastin, or a combination of both. Vinculin was used as loading control. (E) HeLa cells were cells transfected with 50 nM siRNA (siScr negative ctrl or siHO-1). Ferroptosis was induced with 10 μM erastin in the presence or absence of 200 μM I3P and quantified by CellTox staining using the Incucyte device. n = 3 biological replicates; the graph is representative for three independent experiments. All error bars represent standard deviation.

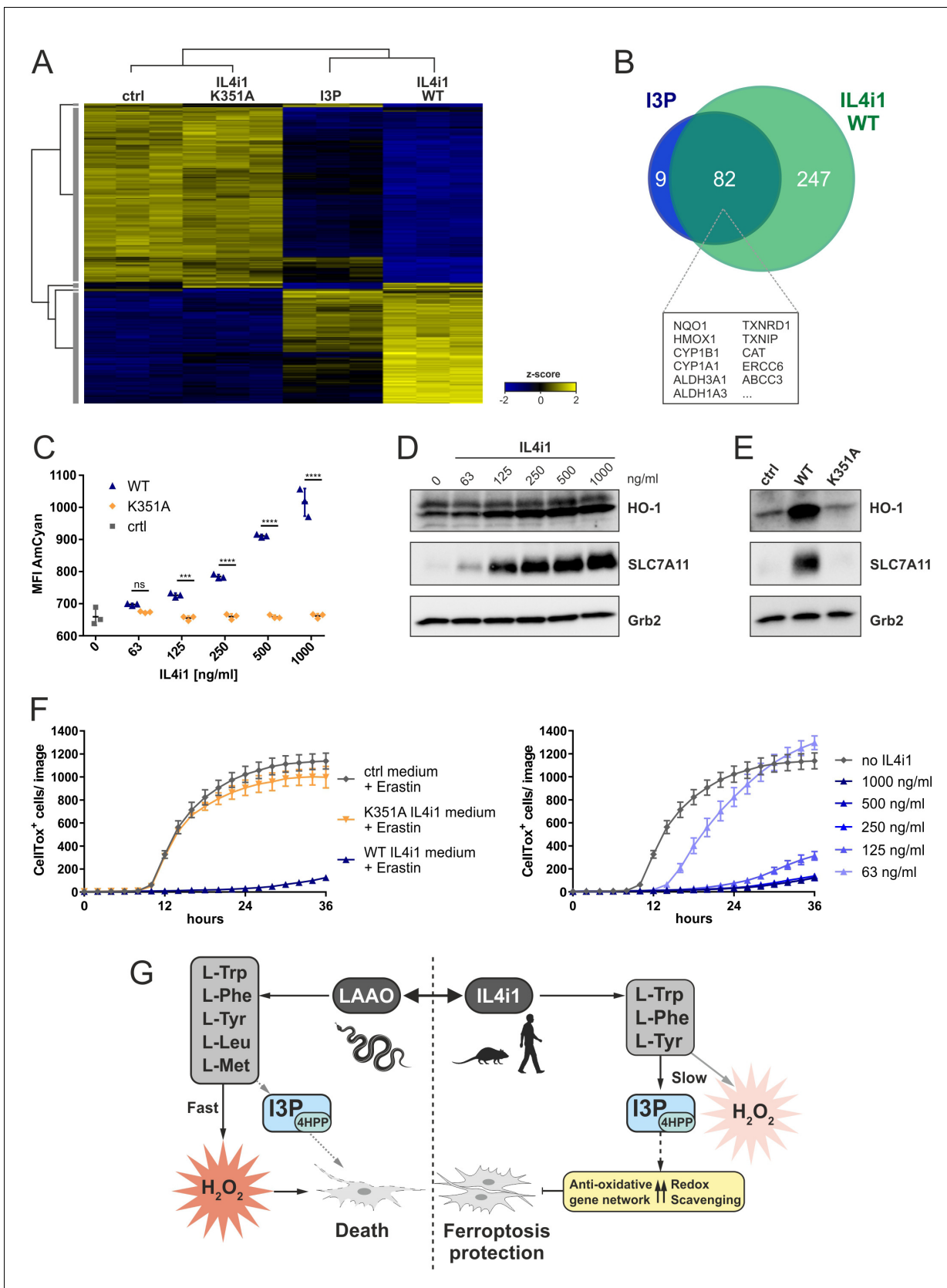


Figure 6. IL4i1 generates an anti-ferroptotic milieu. (A) Heat map of differentially expressed genes in HeLa cells after 24 hr incubation with IL4i1 (WT or K351A inactive mutant [Figure 2—figure supplement 1])-conditioned DMEM, 200 μ M I3P, or untreated control medium. (B) Overlap of most Figure 6 continued on next page

Figure 6 continued

significantly upregulated genes as compared to the untreated HeLa cells (adjusted p-value < 10^{-9}) in HeLa cells treated with I3P and WT IL4i1 conditioned medium. Many of the overlapping genes are associated with Nrf2 and AhR signaling. (C) I3P uptake by HeLa cells was quantified after 24 hr of incubation with IL4i1 conditioned DMEM by flow cytometry. n = 3 biological replicates; the graph is representative for three independent experiments. Data were analyzed by two-way ANOVA with Sidak's multiple comparisons test; ***p < 0.001; ****p < 0.0001; ns = not significant. (D, E) HO-1 or SLC7A11 expression was determined by immunoblotting following transfer of complete DMEM media treated with increasing concentrations of IL4i1 or enzyme-dead K351A mutant for 24 hr. (F) Quantification of erastin-induced ferroptosis in HeLa cells in the presence of IL4i1 conditioned DMEM. WT but not K351A mutant IL4i1 conditioned medium (1 μ g/ml) suppressed ferroptosis (left). The anti-ferroptotic effect of IL4i1 is concentration dependent (right). n = 2 biological replicates; the graphs are representative for three independent experiments. All error bars represent standard deviation. (G) Schematic representation of the death-inducing versus death-protection mechanisms of venom LAAO versus mammalian IL4i1.

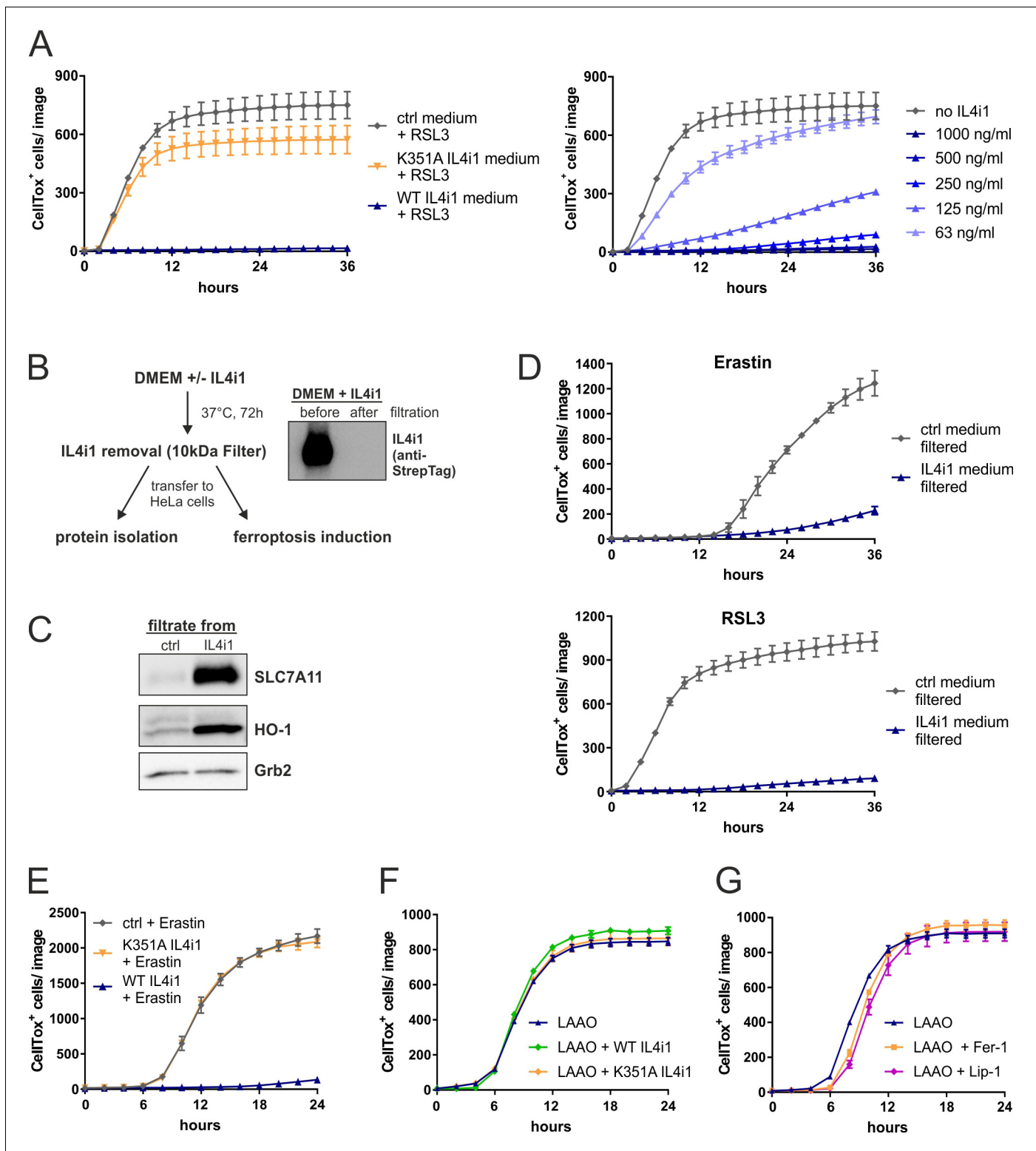


Figure 6—figure supplement 1. IL4i1 generates an anti-ferroptotic milieu. (A) Quantification of RSL3-induced ferroptosis in HeLa cells in the presence of IL4i1 conditioned DMEM. WT but not K351A mutant IL4i1 conditioned medium (1 μ g/ml) suppressed ferroptosis (left). The anti-ferroptotic effect of IL4i1 is concentration dependent (right). $n = 2$ biological replicates; the graphs are representative for three independent experiments. (B) Simplified schema and representative immunoblot of IL4i1 removal by filtration of the conditioned medium using a 10 kDa centrifugal filter. (C) HO-1 and SLC7A11 expression in HeLa cells after 24 hr incubation with filtered DMEM media treated or not treated with recombinant IL4i1 (1 μ g/ml) was analyzed. Figure 6—figure supplement 1 continued on next page

Figure 6—figure supplement 1 continued

by immunoblotting. (D) Filtered DMEM without or treated with recombinant IL4i1 (1 $\mu\text{g/ml}$) was used to quantify ferroptosis suppression of erastin (left) and RSL3 (right) treated HeLa cells ($n = 3$ biological replicates). (E) Quantification of erastin-induced ferroptosis in HeLa cells in the presence of medium with human plasma concentrations of amino acids and glucose. The medium was pre-incubated for 72 hr with IL4i1, transferred to the cells and ferroptosis induced with 1 μM erastin. (F) Quantification of cell death induced by 1.25 $\mu\text{g/ml}$ snake venom LAAO in HeLa cells in the presence of IL4i1 conditioned DMEM. (G) Quantification of cell death induced by 1.25 $\mu\text{g/ml}$ snake venom LAAO in HeLa cells in the presence of the ferroptosis inhibitors ferrostatin-1 (Fer-1, 2 μM) and lipoxstatin-1 (Lip-1, 1 μM). E–G: $n = 3$ biological replicates. The graphs are representative for three independent experiments. All error bars represent standard deviation.